

Overlapping finite elements for a new paradigm of solution



Lingbo Zhang, Klaus-Jürgen Bathe*

Massachusetts Institute of Technology, Cambridge, MA 02139, USA

ARTICLE INFO

Article history:

Received 14 December 2016

Accepted 13 March 2017

Keywords:

Finite elements
Overlapping elements
Meshfree methods
Meshing
Numerical integration of matrices
CAD

ABSTRACT

We present novel overlapping finite elements for a new paradigm of solution proposed in our previous papers, see Bathe (2016) and Bathe and Zhang (2017).

We give the formulation of the new overlapping elements and the solutions of basic numerical examples to investigate the robustness and efficiency of the new finite elements. The results show that the new overlapping elements are quite distortion insensitive and the numerical integration of the element matrices is efficient. The computational effort to integrate the matrices is much less than in meshfree methods. Finally, we illustrate the complete solution scheme of the new paradigm using the overlapping finite elements in the analysis of the bracket problem already considered in Bathe and Zhang (2017).

While the paper proposes and studies new overlapping elements, we conclude that further research is needed to fully harvest the potential of the new analysis approach.

© 2017 Elsevier Ltd. All rights reserved.

1. Introduction

The finite element method is now established as an effective numerical procedure and is much used for the analysis of structures, fluids, and multi-physics problems, see for example [3]. However, despite its great success, the required meshing still presents difficulties. In engineering analyses of complex components, oftentimes, much more time is spent on reaching an adequate mesh than obtaining the solution of the finite element model. In a traditional finite element analysis, the elements must abut each other and cannot overlap, which leads to meshing difficulties and frequently to highly distorted elements that pollute the accuracy of the overall finite element solution.

For these reasons, many meshfree or meshless methods have been developed, see for example Refs. [2,4]. In a meshfree method, the global solution field is constructed using scattered points in the analysis domain without a mesh. Compared with analyses using traditional finite elements, the solutions obtained using a meshfree method may be relatively insensitive to the points or nodes used. Hence the solution accuracy may be improved. However, while the effort to establish the discretization is much less, and good solution accuracy can be obtained, the required numerical integration using a meshfree method is computationally expensive [2,4–9]. This expense largely restricts the wide use of meshless methods in engineering practice.

To improve the accuracy of solutions obtained when using traditional finite elements, specifically when distorted meshes are employed, some researchers have focused on improving the performance of the traditional finite elements by generalizing finite element formulations, see for example [10–13]. In a related approach, interpolation covers were introduced in Refs. [14,15] to obtain improved solution accuracy. Compared with the use of meshfree methods, these schemes are quite efficient in the numerical integration. However, the procedures need a mesh and the solutions are still quite sensitive to mesh distortions, indeed the solution accuracy may decay rapidly when highly distorted elements are used.

To significantly improve the meshing procedures of geometrically complex solids, we proposed a new paradigm for CAD driven simulations [1,2]. In the new approach, the CAD part is immersed in a Cartesian grid of uniform cells determined by the analyst, the boundary of the part is discretized, and the cells within the analysis domain of the CAD part are automatically, and with very little computational effort, converted to traditional finite elements. Thereafter, overlapping finite elements are used along the boundaries of the part to fill-in the empty space and couple with the traditional finite elements.

In the new paradigm of solution, the meshing, including the clean-up of the geometry, is embedded into CAD driven solutions. Undistorted finite elements are used in the inner part of the analysis domain and overlapping elements are used on and near the boundaries. Hence, provided the overlapping finite elements perform well, the scheme does not have an element distortion problem, and compared with meshfree methods, the computational

* Corresponding author.

E-mail address: kjb@mit.edu (K.J. Bathe).

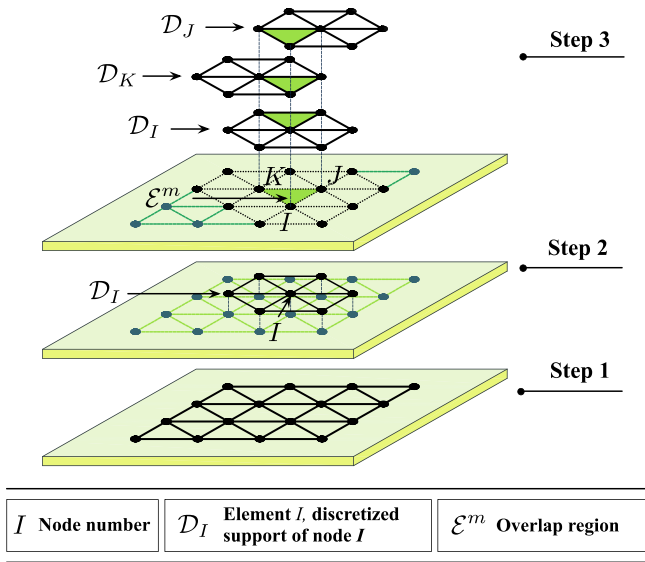


Fig. 1. Schematic of elements corresponding to $\mathcal{D}_I, \mathcal{D}_J, \mathcal{D}_K$ using triangular regions; the local fields are constructed for the support of each node I, J, K ; the global field is built from the local fields.

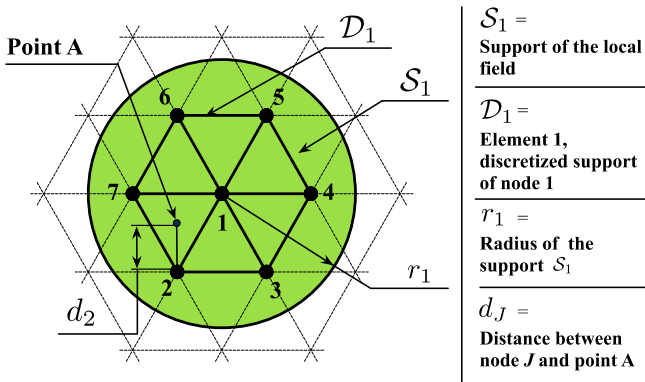


Fig. 2. Schematic of the 7-node element 1, or discretized support \mathcal{D}_1 .

time is much less because overlapping elements are only used near the boundaries.

In Ref. [2] we used the spheres of the method of finite spheres [16,17] as overlapping elements, and also pointed out that other

overlapping elements could be used. Clearly, to fully harvest the potential of the given analysis approach, efficient overlapping elements are needed.

Our objective in this paper is to present new robust and efficient overlapping finite elements that satisfy the consistency requirements and use much less integration points, and hence are, for example, much more efficient than those in Refs. [2,18]. In Section 2, we give the basic theory of the new overlapping elements including the theory for coupling the overlapping elements to the traditional finite elements. Then in Section 3, we discuss the solutions of four numerical examples in which we compare the performance of the new overlapping elements with the performance of the method of finite spheres [16,17] and the finite element method enriched by interpolation covers [14,15]. Thereafter, to illustrate the complete solution scheme of the new paradigm for analysis using the new overlapping elements, we revisit in Section 4 the analysis of the bracket already considered in Ref. [2]. Finally, we present our conclusions in Section 5.

2. The overlapping finite elements

Our objective in this section is to present the theoretical formulation of the new overlapping elements including the theory for coupling these with the traditional finite elements, the imposition of the Dirichlet boundary conditions and the numerical integration used for the element matrices.

2.1. The interpolations used for the overlapping finite elements

Effective overlapping elements should show two important properties. Firstly, the integration of the element stiffness matrices should be computationally efficient, and secondly, the overlapping elements should be distortion-insensitive. In order to develop overlapping elements that show both properties, we propose a new scheme for the local and global approximation fields. Considering Fig. 1, there are three major steps.

The first step is to discretize “the region” in the usual way. We use here 3-node triangular elements but other elements could also be used. In the new paradigm of solution, the region considered is the space between the boundary of the discretized CAD part and the Cartesian mesh of traditional finite elements [2]. The second step is to construct the local field within the support of each node. The local analysis domain \mathcal{D}_I (in Fig. 1, given by the union of the 6 triangular regions) denotes the support of node I , and we refer to it as element I . In order for the scheme to be quite distortion insensitive, the local field is constructed as discussed in Section 2.1.1.

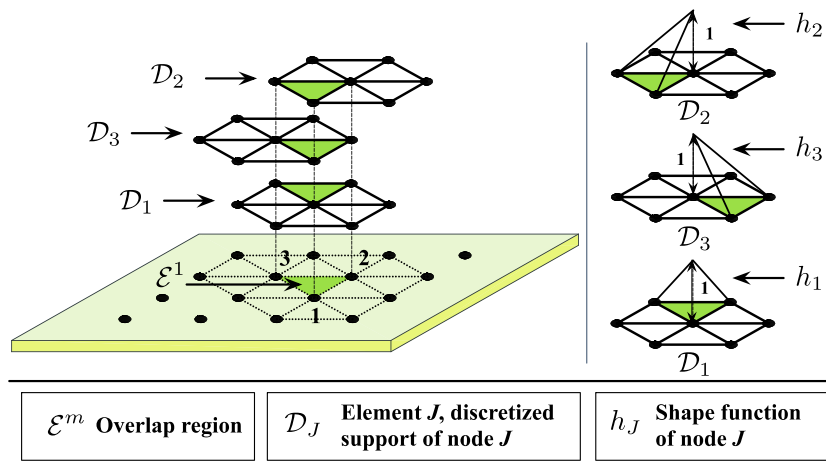


Fig. 3. Schematic of the interpolation process in the overlap region \mathcal{E}^1 .

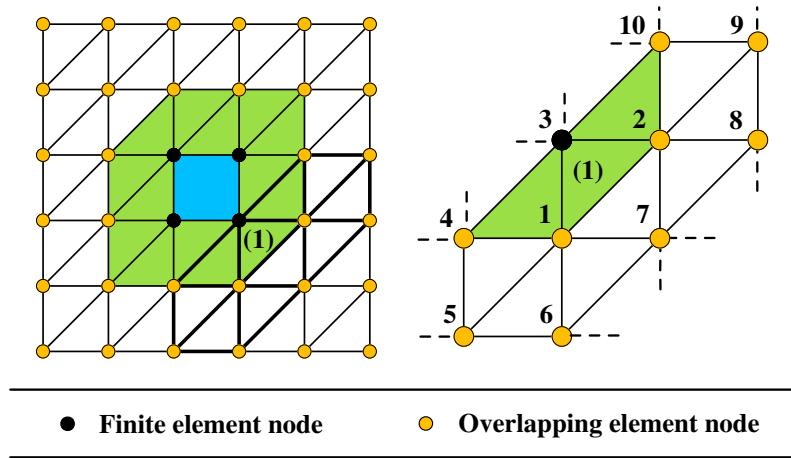


Fig. 4. A schematic mesh generated with the new meshing scheme; the green elements denote the coupling regions (here 3-node triangular regions) and the blue element represents the 4-node traditional finite element.

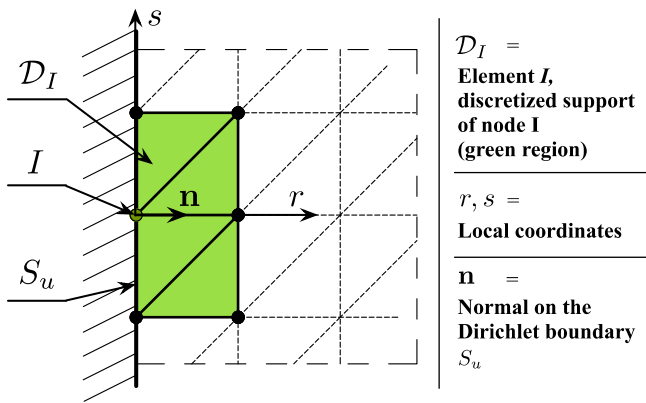


Fig. 5. A typical Dirichlet boundary S_u .

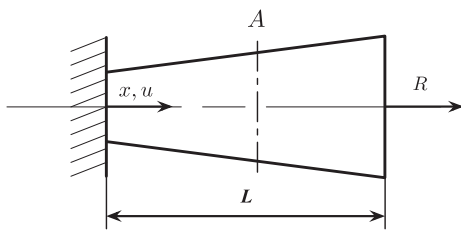


Fig. 6. An elastic bar with varying cross section ($L = 5$, $E = 200 \times 10^9$, $R = 1000$, $A = 1 + x$).

In the third step the global approximation field is established. The global field is built from the local fields using the partition of unity. For example, in the overlap region \mathcal{E}^m (see step 3, in Fig. 1), given by the three overlapping 7-node elements (each discretized by six 3-node regions which look like traditional finite elements), the global field is obtained from the local overlapping fields in \mathcal{D}_I , \mathcal{D}_J , and \mathcal{D}_K . The details are given in Section 2.1.2.

2.1.1. Local interpolation

Let \mathcal{N}_I be the set of nodes contained in \mathcal{D}_I

$$\mathcal{N}_I := \{M : \mathcal{D}_M \cap \mathcal{D}_I \neq \emptyset\} \tag{1}$$

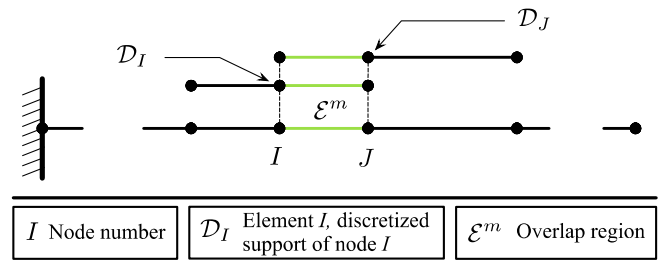


Fig. 7. A mesh of overlapping elements.

where M denotes a node number. Consider a sphere S_I with center at node I and containing all nodes in \mathcal{N}_I .

In the domain S_I , the local field is assumed to be

$$\Psi_I(\mathbf{x}) = \sum_{J \in \mathcal{N}_I} \sum_{n \in \mathbb{N}} \varphi_J^n(\mathbf{x}) (p_n \mathbf{a}_{Jn}) \tag{2}$$

with $\varphi_J^n(\mathbf{x})$ given as

$$\varphi_J^n(\mathbf{x}) = \frac{W_J^n(\mathbf{x})}{\sum_{K \in \mathcal{N}_I} W_K^n(\mathbf{x})} \tag{3}$$

where $W_J^n(\mathbf{x})$ is the weight function of node J . In Eq. (2), p_n denotes the n th polynomial term of the node J in

$$\mathbf{p}^T = [1 \ x \ y \ x^2 \ xy \ \dots] \tag{4}$$

Here, the coordinate variables (x, y) are measured from node J , with the origin of the coordinate system located at node J . We can include in \mathbf{p} higher order terms or special functions to improve the accuracy of the local interpolation. In Eq. (2), $\mathbf{a}_{Jn} = [a_{Jn}^u \ a_{Jn}^v]$ represents the unknown nodal variables.¹

For Eq. (3) the weight function is chosen as

$$W_J^n(\mathbf{x}) = \begin{cases} 1 - 6s^2 + 8s^3 - 3s^4 & 0 \leq s \leq 1 \\ 0 & s > 1 \end{cases} \tag{5}$$

with s given by

$$s = \frac{d_J}{2r_I} \tag{6}$$

¹ While in our earlier papers for spheres/disks, we employed the symbol α_{jn} to indicate the unknowns, we use now, including the coupling, the symbol \mathbf{a}_{jn} .

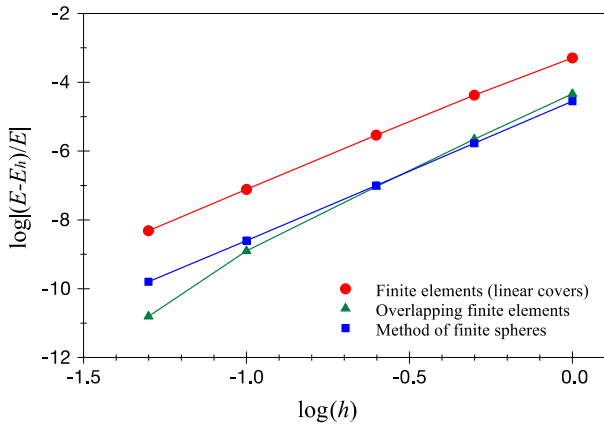


Fig. 8. Convergence of the calculated strain energy E_h using various methods.

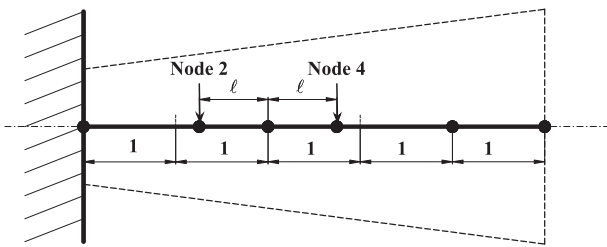


Fig. 9. The mesh for the element distortion study; element quality decreases as the distance ℓ decreases.

where d_j denotes the distance between node J and point $\mathbf{x} = (x, y)$, and r_i is the radius of S_i . This radius is selected to contain all nodes listed in \mathcal{N}_i . For an example see Fig. 2 in which $I = 1$.

From Eq. (2), the local field contribution from the solution variables of nodes in \mathcal{N}_1 is expressed as

$$\begin{aligned} \psi_1(\mathbf{x}) &= \sum_{J \in \mathcal{N}_1} \sum_{n \in \mathcal{N}_3} \varphi_J^1(\mathbf{x})(p_n \mathbf{a}_{Jn}) \\ &= \sum_{J \in \mathcal{N}_1} \left(\frac{W_J^1(\mathbf{x})}{\sum_{K \in \mathcal{N}_1} W_K^1(\mathbf{x})} (\mathbf{a}_{J1} + \mathbf{a}_{J2}x + \mathbf{a}_{J3}y + \mathbf{a}_{J4}x^2 + \mathbf{a}_{J5}xy + \dots) \right) \end{aligned} \quad (7)$$

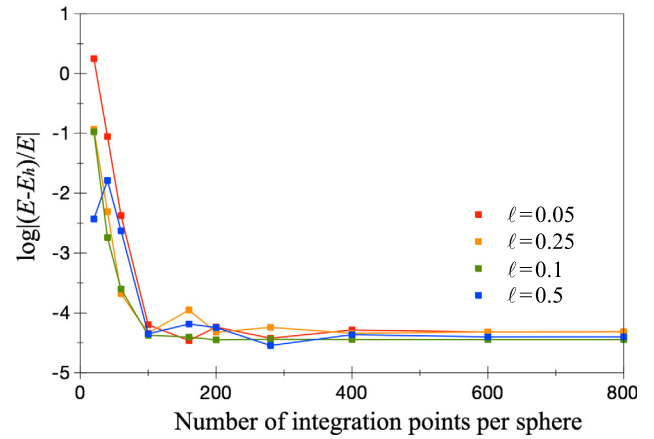


Fig. 11. Solution accuracy of the method of finite spheres as a function of the number of integration points per sphere; the same order composite Gauss integration rule is employed for all spheres.

where in Fig. 2 $\mathcal{N}_1 = \{1, 2, 3, 4, 5, 6, 7\}$. As shown in Eq. (7), the local field $\psi_1(\mathbf{x})$ contains contributions from all nodes in \mathcal{N}_1 .

2.1.2. Global interpolation

Let $\{\mathcal{T}_h\} := \{\mathcal{E}^m\}_{m=1}^e$ be the e triangular overlap regions that together discretize the global analysis domain Ω

$$\bigcup_{m=1}^e \mathcal{E}^m = \Omega \quad (8)$$

Let I_m be the set of indices defined by

$$I_m := \{I : \mathcal{D}_I \cap \mathcal{E}^m \neq \emptyset\} \quad (9)$$

In the overlap region of the three overlapping elements, the global field is constructed from the local fields based on the partition of unity

$$\mathbf{u}(\mathbf{x}) = \sum_{m=1}^e \sum_{I \in I_m} h_I \psi_I(\mathbf{x}) = \sum_{m=1}^e \sum_{I \in I_m} h_I \left(\sum_{J \in \mathcal{N}_1} \sum_{n \in \mathcal{N}_3} \varphi_J^1(\mathbf{x})(p_n \mathbf{a}_{Jn}) \right) \quad (10)$$

where $\psi_I(\mathbf{x})$ is the local field corresponding to node I (see Eqs. (2)–(6)) and h_I is the partition of unity function of node I , equal to the

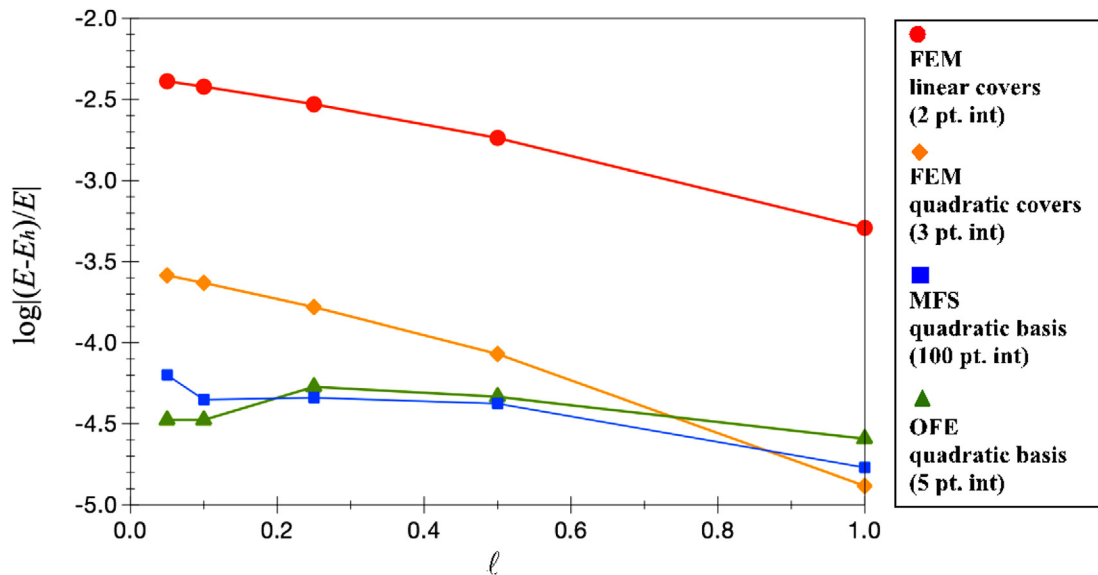


Fig. 10. Element distortion study with various methods. Using the overlapping elements (OFE), elements with covers, and the method of finite spheres (MFS).

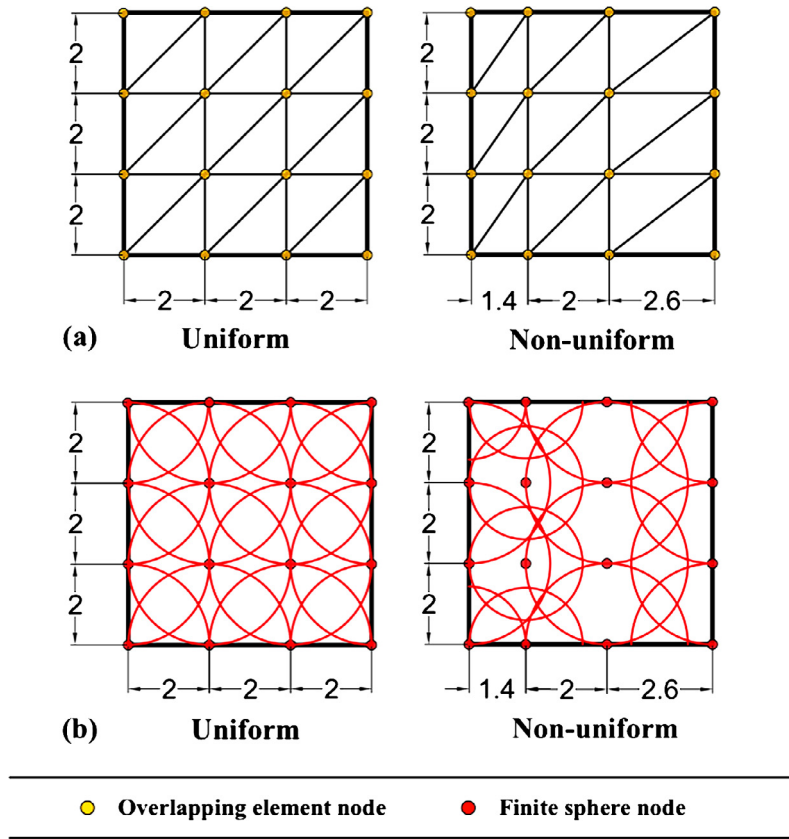


Fig. 12. The patch of elements; plate in plane strain conditions subjected to normal stresses $\tau_{xx} = 2.0$, $\tau_{yy} = 2.0$ (Length = 6, thickness = 1, $E = 100$, $\nu = 0.3$); (a) the mesh of the overlapping elements; (b) the finite spheres, here disks; in each case, the linear polynomial basis is used.

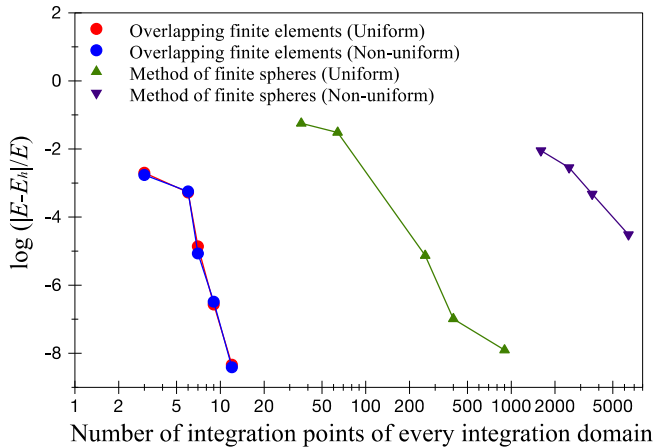


Fig. 13. The accuracy of the strain energy as a function of the number of integration points used for each integration domain; using the overlapping elements the integration domain is the triangular overlap region, in the method of finite spheres, the domain is the disk.

nodal shape function of the traditional triangular finite element. We note that in this formulation the regions \mathcal{D}_i , \mathcal{D}_j , \mathcal{D}_k are the overlapping elements with \mathcal{E}^m the region that is overlapped, see Fig. 1, and that the displacement field thus constructed is continuous.

From Eq. (10), the global field in \mathcal{E}^m is given as

$$\mathbf{u}(\mathbf{x}) = \sum_{M \in \mathcal{I}_m} h_M \Psi_M(\mathbf{x}) = h_I \Psi_I(\mathbf{x}) + h_J \Psi_J(\mathbf{x}) + h_K \Psi_K(\mathbf{x}) \quad (11)$$

We present an example in Fig. 3, with $I = 1$, $J = 2$, $K = 3$, $m = 1$, where also the partition of unity functions h_1, h_2, h_3 are shown. This example also shows how local nodes are used in the calculation, to obtain as usual the global contributions to the matrices of the element assemblage [5].

2.2. Coupling with traditional finite elements

In the new paradigm of solution [2], the complete analysis domain is first immersed in a grid determined by the analyst. Then the cells located entirely within the analysis domain are automatically converted to traditional finite elements. Thereafter, the overlapping elements are used along the boundaries to cover the otherwise empty space and extended to couple with the traditional finite elements. Fig. 4 shows schematically a simple mesh generated for an in-plane problem with the new meshing scheme.

The coupling between the overlapping elements and the finite elements is presented in our previous paper [2]. Using the local node numbering, the displacement field within a 3-node triangular overlap region (next referred to as “element”) is given as

$$\mathbf{u}(\mathbf{x}) = \sum_{I \in \mathcal{X}} h_I \left(h_I \mathbf{u}_I + \sum_{\substack{K \in \mathcal{K} \\ K \neq I}} h_K \mathbf{a}_{K1} \right) + \sum_{I=1}^{noe} h_I \hat{\Psi}_I \quad (12)$$

where \mathcal{X} is the index set of the pure finite element nodes of the element in the coupling region considered, h_I is the shape function of node I of the traditional finite element, \mathcal{K} is the index set of all nodes of the element, noe is the number of overlapping elements which have an intersection with the element in the coupling region,

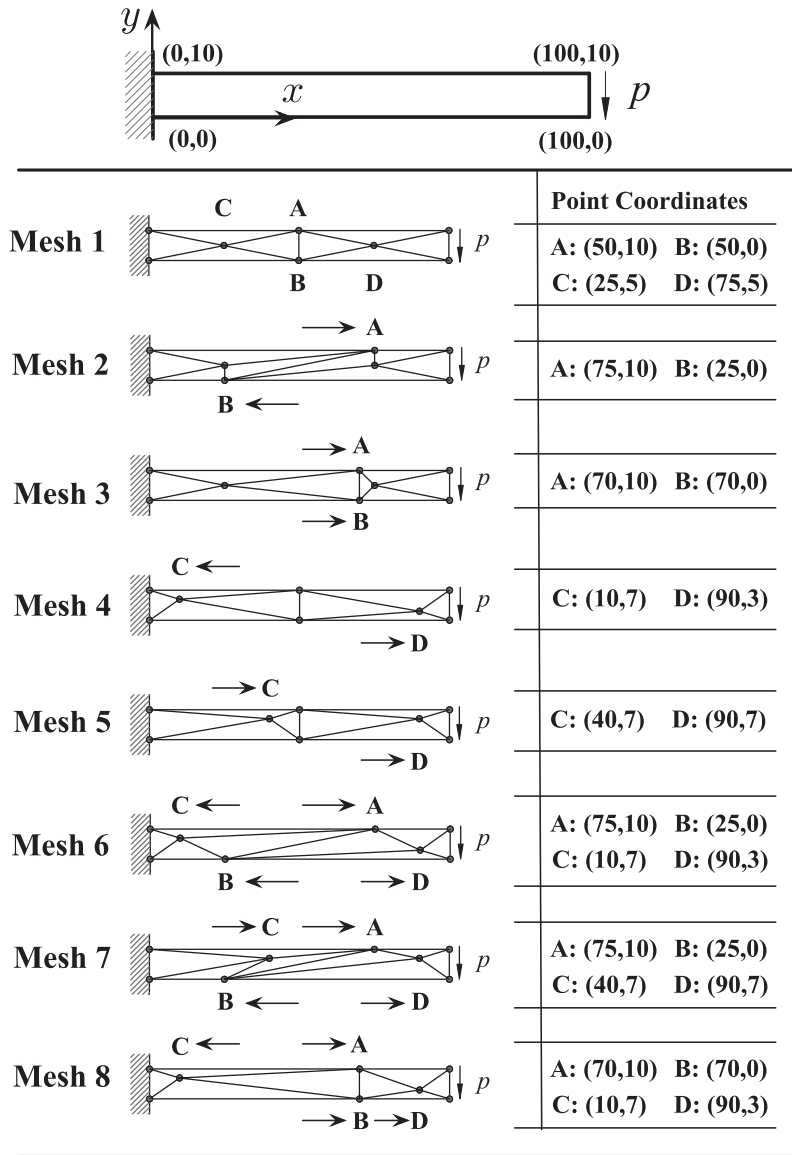


Fig. 14. Eight meshes used in the analysis of a cantilever beam problem; plane strain conditions, thickness = 1, $p = 100$, $E = 200 \times 10^7$, $\nu = 0.3$.

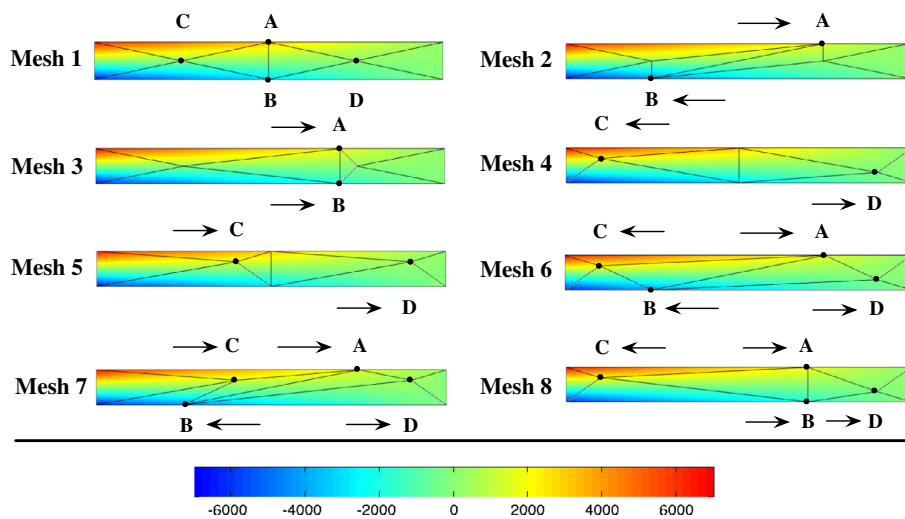


Fig. 15. Stress plots (non-smoothed) of the longitudinal stress τ_{xx} for the 8 distorted meshes used.

Table 1
Numerical results (rounded) at selected points of the cantilever beam problem.

	Mesh 1	Mesh 2	Mesh 3	Mesh 4	Reference solution
$\tau_{xx}(50, 10)$	2922	2770	3043	3193	3003
ϵ_h	2.7%	7.8%	1.3%	6.3%	
$\tau_{xx}(50, 0)$	-2922	-3163	-3043	-3076	-3003
ϵ_h	2.7%	5.3%	1.3%	2.4%	
$\delta(100, 10)$	-1.80E-3	-1.80E-3	-1.80E-3	-1.81E-3	-1.83E-3
ϵ_h	1.4%	1.7%	1.7%	1.03%	
E_h	0.902	0.899	0.899	0.905	0.915
ϵ_h	1.4%	1.7%	1.7%	1.02%	
	Mesh 5	Mesh 6	Mesh 7	Mesh 8	Reference solution
$\tau_{xx}(50, 10)$	3084	3007	2607	2992	3003
ϵ_h	2.7%	0.1%	13.2%	0.4%	
$\tau_{xx}(50, 0)$	-3050	-2861	-3077	-3026	-3003
ϵ_h	1.5%	4.7%	2.4%	0.7%	
$\delta(100, 10)$	-1.79E-3	-1.81E-3	-1.79E-3	-1.81E-3	-1.83E-3
ϵ_h	2.0%	1.0%	2.0%	1.2%	
E_h	0.897	0.905	0.896	0.904	0.915
ϵ_h	2.0%	1.0%	2.0%	1.2%	

Percent error $\epsilon_h = 100\% \times \frac{|\eta_h - \eta|}{\eta}$; η_h denotes the numerical result and η is the reference solution which is obtained using a 100×1000 element mesh of 9-node finite elements, δ denotes the transverse displacement.

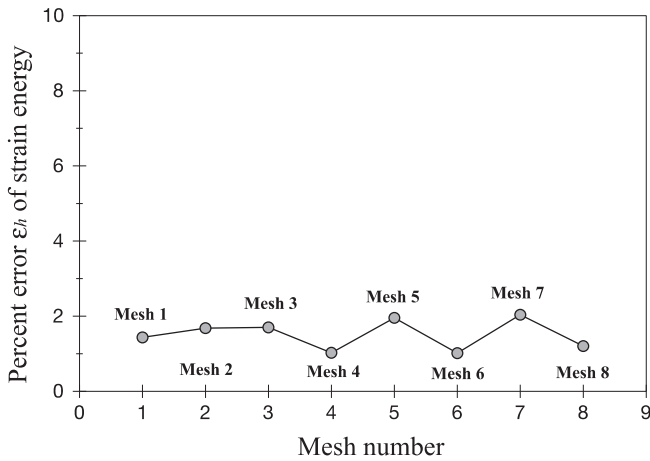


Fig. 16. Percent error ϵ_h of the strain energy obtained using the overlapping elements.

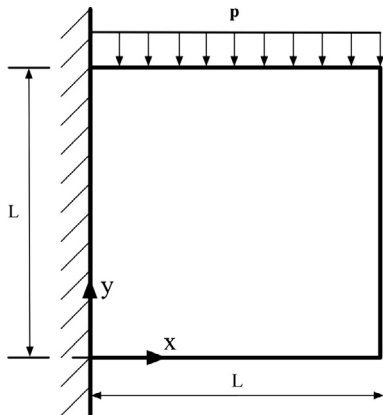


Fig. 17. A cantilever plate in plane strain conditions subjected to a uniformly distributed load, $p = 1.0$ per unit length (thickness = 1.0, $L = 2.0$, $E = 100$, $\nu = 0.3$).

$$\hat{\psi}_I(\mathbf{x}) = \sum_{\substack{J \in \mathcal{N}_I \\ J \neq I}} \varphi_J^I(\mathbf{x}) \sum_{n \in \mathcal{N}} (p_n \mathbf{a}_{Jn}) + \sum_{J \in \mathcal{X}} \varphi_J^I(\mathbf{x}) \left(\sum_{K \in \kappa} h_K \mathbf{a}_{K1} \right) \quad (13)$$

where $\mathbf{a}_{K1} = [a_{K1}^u \ a_{K1}^v]$ is the unknown solution vector of node K , equal to \mathbf{u}_K .

The resulting field satisfies the rigid body mode conditions and the patch test, see Ref. [2]. For the coupling region (1) in Fig. 4, we have two overlapping elements 1 and 2, identified through their center nodes 1 and 2, and the index sets used in Eqs. (12) and (13) are $\kappa = \{1, 2, 3\}$ and $\mathcal{X} = \{3\}$, respectively, with $\mathcal{N}_1 = \{1, 2, 3, 4, 5, 6, 7\}$ and $\mathcal{N}_2 = \{1, 2, 3, 7, 8, 9, 10\}$. Of course, the local nodes used here are related to the global nodes as usual for the assemblage process [5].

2.3. Governing equations in linear elastic solid mechanics

Using the general principle of virtual work [5], as in traditional finite element analysis, we have

$$\int_{\Omega} \bar{\boldsymbol{\epsilon}}^T \boldsymbol{\tau} \, d\Omega = \int_{\Omega} \bar{\mathbf{u}}^T \mathbf{f}^B \, d\Omega + \int_{S_f} \bar{\mathbf{u}}^{S_f T} \mathbf{f}^{S_f} \, dS \quad (14)$$

where $\boldsymbol{\epsilon}$ is the strain vector, $\boldsymbol{\tau}$ is the stress vector, \mathbf{u} is the displacement vector (which satisfies the essential boundary conditions), \mathbf{f}^B is the body force, and \mathbf{f}^{S_f} is the prescribed surface traction vector on the boundary S_f . An overbar denotes a virtual quantity.

In elastic solid mechanics, the stress-displacement relation is given as

$$\boldsymbol{\tau} = \mathbf{C} \boldsymbol{\epsilon}(\mathbf{u}) \quad (15)$$

where \mathbf{C} is the stress-strain matrix, $\boldsymbol{\epsilon}(\mathbf{u})$ is the strain, a function of \mathbf{u} . From Eq. (10), the displacement formulation of the overlapping elements could be expressed as

$$\mathbf{u} = \sum_{m=1}^e \sum_{l \in I_m} h_l \psi_l = \sum_{l=1}^N \sum_{n \in \mathcal{N}} \mathbf{H}_{ln} \mathbf{a}_n \quad (16)$$

where N is the total number of applicable nodes, \mathbf{H}_{ln} denotes the displacement interpolation matrix corresponding to the n th degree of freedom at node l , $\mathbf{a}_n = [a_{ln}^u \ a_{ln}^v]$ is the vector of unknowns of node l corresponding to n . The strain-displacement function $\boldsymbol{\epsilon}(\mathbf{u})$ is

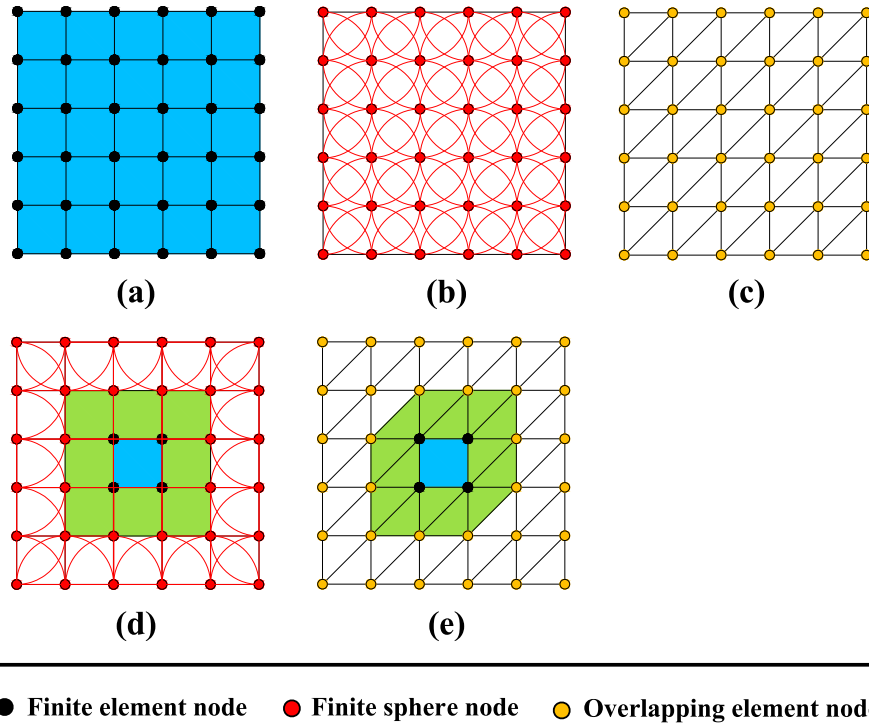


Fig. 18. The discretizations using the various schemes; (a) 4-node traditional finite elements (2×2 Gauss integration); (b) method of finite spheres (MFS) with bilinear basis (24×24 Gauss integration); (c) overlapping elements only, with bilinear basis (OFE) (9-point integration); (d) new meshing scheme with MFS and hat functions for the coupling (for red nodes on the boundary) [2]; (e) new meshing scheme with OFE; the green zones represent the coupling regions and the blue zones denote the traditional 4-node finite elements.

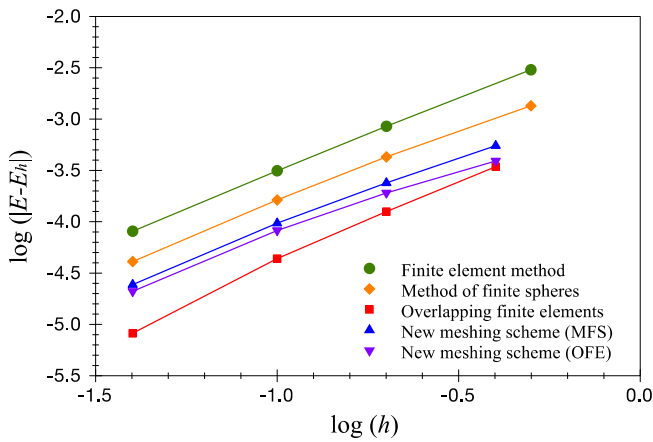


Fig. 19. Convergence of the strain energy in the analysis of the cantilever plate using various methods. The reference strain energy E is obtained using a 100×100 element mesh of traditional 9-node finite elements.

$$\boldsymbol{\varepsilon}(\mathbf{u}) = \sum_{I=1}^N \sum_{n \in \mathcal{S}} \mathbf{B}_{In} \mathbf{a}_{In} \quad (17)$$

where \mathbf{B}_{In} denotes the strain interpolation matrix corresponding to the n th degree of freedom at node I . From Eqs. (14)–(17), with the usual procedure in finite element analysis, we obtain

$$\mathbf{K} \mathbf{a} = \mathbf{R} \quad (18)$$

where the vector of unknown solution variables is

$$\mathbf{a}^T = [\mathbf{a}_{11} \ \mathbf{a}_{12} \ \dots \ \mathbf{a}_{21} \ \mathbf{a}_{22} \ \dots \ \mathbf{a}_{N1} \ \mathbf{a}_{N2} \ \dots \ \mathbf{a}_{Nm}] \quad (19)$$

where m is the number of terms included in \mathbf{p} and \mathbf{K} is the stiffness matrix and \mathbf{R} is the load vector. Inertia and damping effects could be

included as usual [5]. The expressions for the stiffness matrix \mathbf{K} and the load vector \mathbf{R} are for node I and degree of freedom m of the form

$$\sum_{J=1}^N \sum_{n \in \mathcal{S}} \mathbf{K}_{ImJn} \mathbf{a}_{Jn} = \mathbf{f}_{Im}^B + \mathbf{f}_{Im}^S \quad (20)$$

where for the stiffness matrix

$$\mathbf{K}_{ImJn} = \int_{V_I} \mathbf{B}_{Im}^T \mathbf{C} \mathbf{B}_{Jn} dV \quad (21)$$

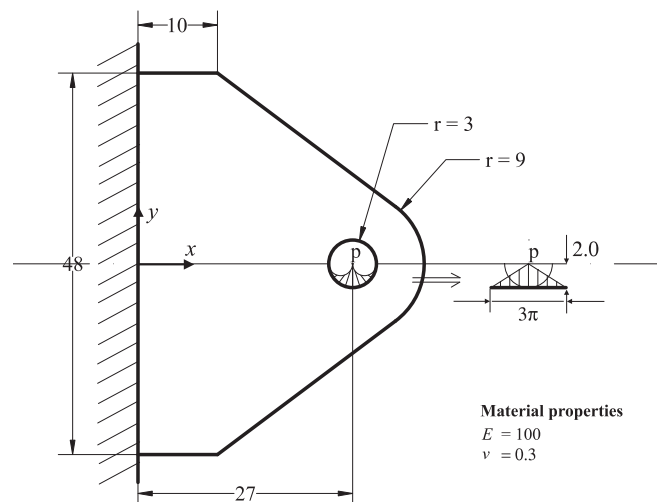


Fig. 20. Geometry of bracket as obtained from the CAD program (unit thickness).

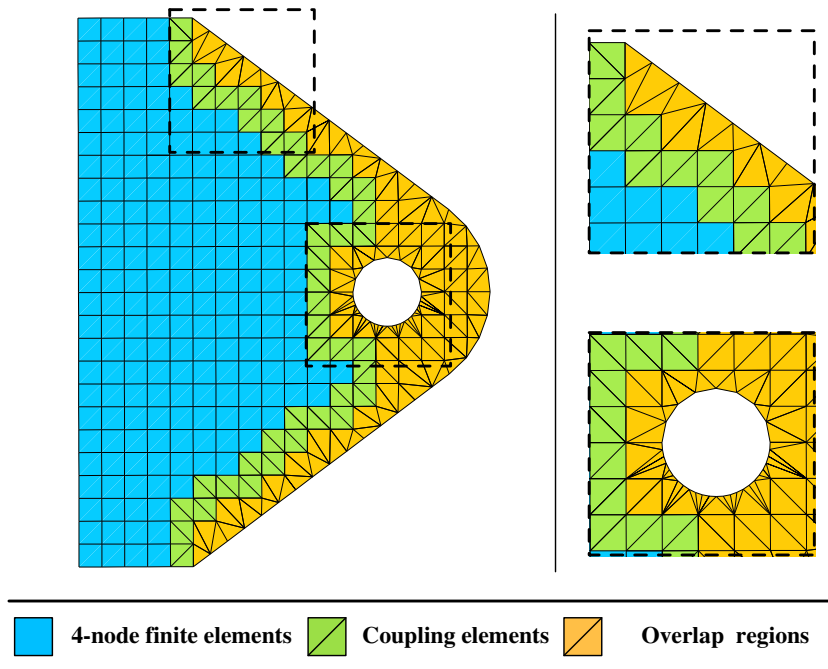


Fig. 21. The mesh of the new scheme in the analysis of the bracket. In the overlapping elements, the bilinear polynomial basis is used.

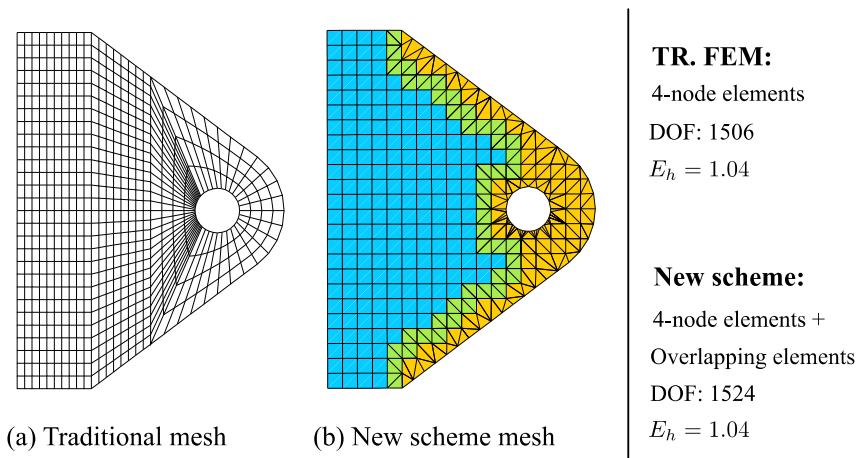


Fig. 22. The meshes of the traditional finite method using 4-node elements and the new scheme; for the overlapping elements, the bilinear polynomial basis is used with 6-point integration; for the traditional finite elements 2×2 Gauss integration is used.

the body force load vector

$$\mathbf{f}_{lm}^B = \int_{V_l} \mathbf{H}_{lm} \mathbf{f}^B dV \quad (22)$$

and the traction force vector

$$\mathbf{f}_{lm}^{S_f} = \int_{S_{f_l}} \mathbf{H}_{lm} \mathbf{f}^{S_f} dS \quad (23)$$

with $V_l = \bigcup_{J \in \mathcal{N}_l} \mathcal{D}_J$ and $S_{f_l} = S_f \cap \mathcal{D}_l$.

Similarly, the contributions from the elements in the coupling regions are evaluated.

2.4. Imposition of the Dirichlet boundary conditions

To impose the Dirichlet boundary conditions we simply place the nodes of the overlapping elements along the boundary and reconstruct the local field using interpolation covers [14]

$$\psi_l(\mathbf{x}) = \sum_{n \in \mathcal{N}_l} p_n \mathbf{a}_{ln} \quad (24)$$

in which \mathbf{p} is constructed to automatically set (or be able to set) the relevant degrees of freedom to the appropriate values.

Fig. 5 shows a typical Dirichlet boundary where

$$\mathbf{u}(\mathbf{x}) = \mathbf{0}, \quad \text{for } \mathbf{u} \text{ on } S_u \quad (25)$$

Table 2

Analysis of the bracket example: comparison of the total number of degrees of freedom (DOF), calculated strain energy and total number of integration points.

Meshing scheme	DOF	Strain energy	Total number of integration points
Mesh, 4-node elements	1506	1.04	2848
New meshing scheme	1524	1.04	2276

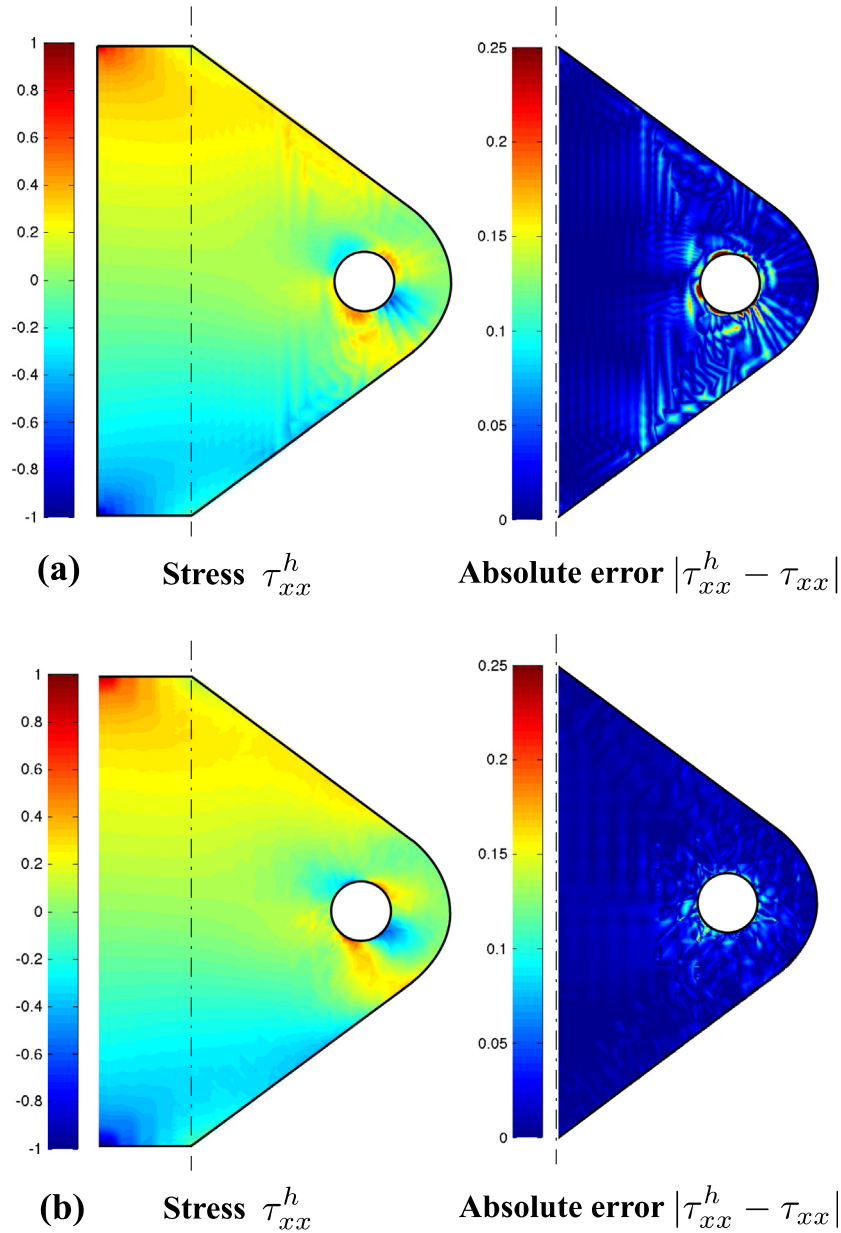


Fig. 23. Stress τ_{xx}^h and absolute error $|\tau_{xx}^h - \tau_{xx}|$; (a) 4-node finite element mesh; (b) new scheme mesh.

Using the r coordinate aligned with the normal \mathbf{n} on the Dirichlet boundary S_u , the vector \mathbf{p} is expressed as

$$\mathbf{p}^T = [r \ r^2 \ rs \ r^3 \ \dots] \quad (26)$$

As we could see from Eqs. (24) and (26), with the new vector \mathbf{p} , the local field is automatically zero at $r = 0$, i.e. on S_u .

2.5. Numerical evaluation of element matrices

The expensive numerical spatial integration is the major difficulty in the use of meshfree methods. The order of integration to be used can be highly dependent on the node distributions and the computational cost can increase significantly when nodes are distributed non-uniformly. The expense in the numerical integration is mainly due to the fact that the overlap regions and the functions therein must be integrated with sufficient accuracy [6]. Using the new overlapping elements, the overlap regions are easily identified and the numerical integration is much more effective. Hence we simply use the commonly employed integration rules for tradi-

tional triangular elements [5]. For the new overlapping elements, we usually use, in two-dimensional analyses, 9-point integration (or even 6-point integration with the bilinear basis) which we so far found to lead to reliable results. We give below a brief study of the effect of the integration orders in the illustrative solutions.

3. Illustrative solutions of problems

In this section, we investigate the properties of the new overlapping elements through the solutions of several numerical examples. We are mainly interested in the effort required in the numerical integration and the element performance when the elements are distorted. We also show the application in the new paradigm of solution proposed in our previous paper [2].

3.1. An elastic bar of varying cross-section

We first consider an elastic bar with varying cross-section, see Fig. 6. The objective is to study the solution convergence of the

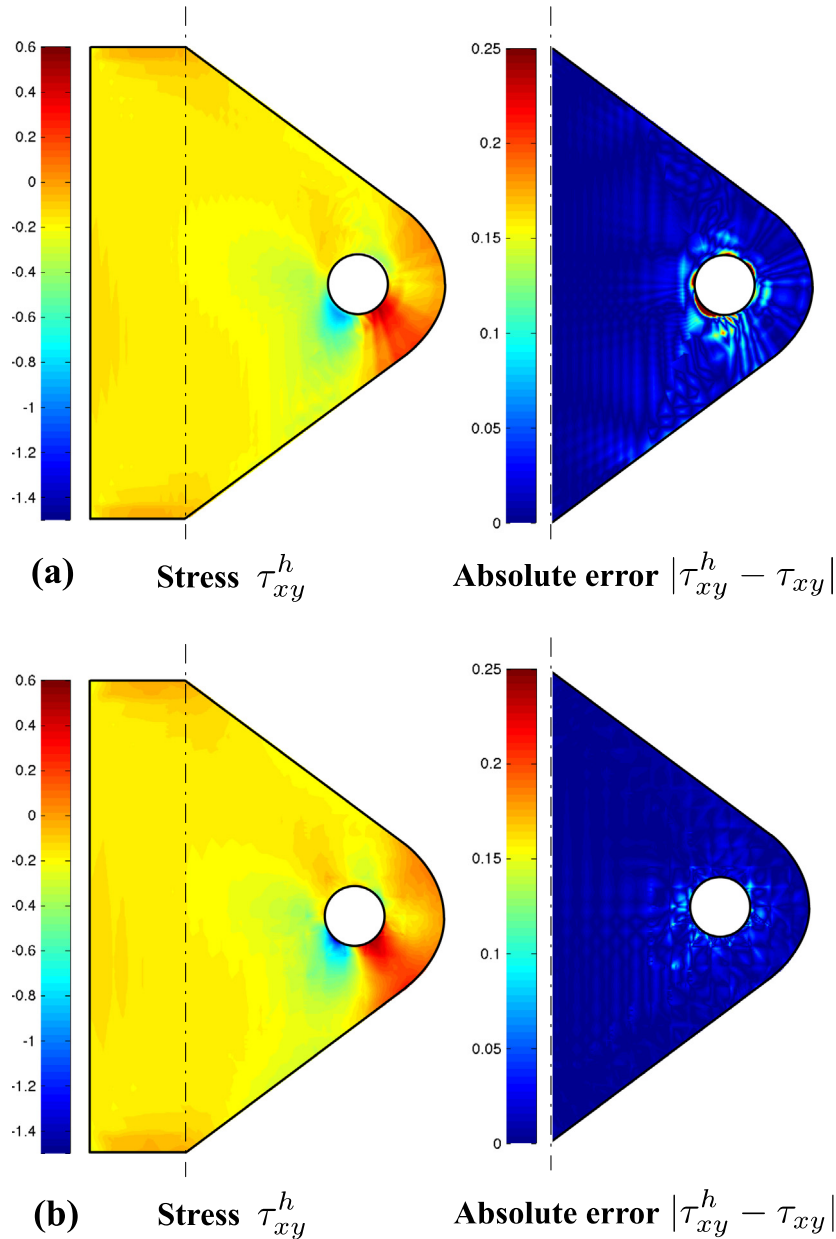


Fig. 24. Stress τ_{xy}^h and absolute error $|\tau_{xy}^h - \tau_{xy}|$; (a) 4-node finite element mesh; (b) new scheme mesh.

new scheme, the finite element method enriched by interpolation covers [14,15] and the method of finite spheres [16,17].

The analytical solution of the response is

$$u = \frac{\ln(1+x)}{2 \times 10^8} \quad 0 \leq x \leq 5 \quad (27)$$

with the resulting strain energy

$$\int_0^5 \frac{1}{2} EA \left(\frac{du}{dx} \right)^2 dx = \frac{\ln(6)}{4} \times 10^{-5} \quad (28)$$

We study the convergence of the strain energy when all methods can theoretically reproduce a quadratic displacement field. The finite element method reproduces the quadratic polynomial displacement field when enriched by linear interpolation covers [14], the method of finite spheres reproduces the quadratic field when the quadratic polynomial basis is used [16], and the overlapping elements reproduce the quadratic field when the quadratic

polynomial basis is used in Eq. (4). Fig. 7 shows typical overlapping elements. For the overlapping elements and the finite elements enriched by linear/quadratic covers we use the standard Gauss quadrature rule for one-dimensional analysis, and 5-point and 2-point/3-point integration respectively [5]. For the method of finite spheres we use a composite Gauss integration rule, the domain of integration (here the “one-dimensional sphere”) is divided into equal parts and for each part 4-point Gauss integration is used, with a total of 100 integration points per domain.

Fig. 8 presents the convergence of the strain energy when h-type uniform refinement is performed. The theoretical order of convergence is 4, which all schemes show, but the overlapping elements perform slightly best.

We next study the effect of a mesh distortion. Fig. 9 shows the specific mesh used. The elastic bar is first discretized using 6 equally spaced nodes where ℓ denotes the distance between the nodes. To introduce a distortion in the mesh, we move nodes 2 and 4 to decrease the distance ℓ between them. The solution

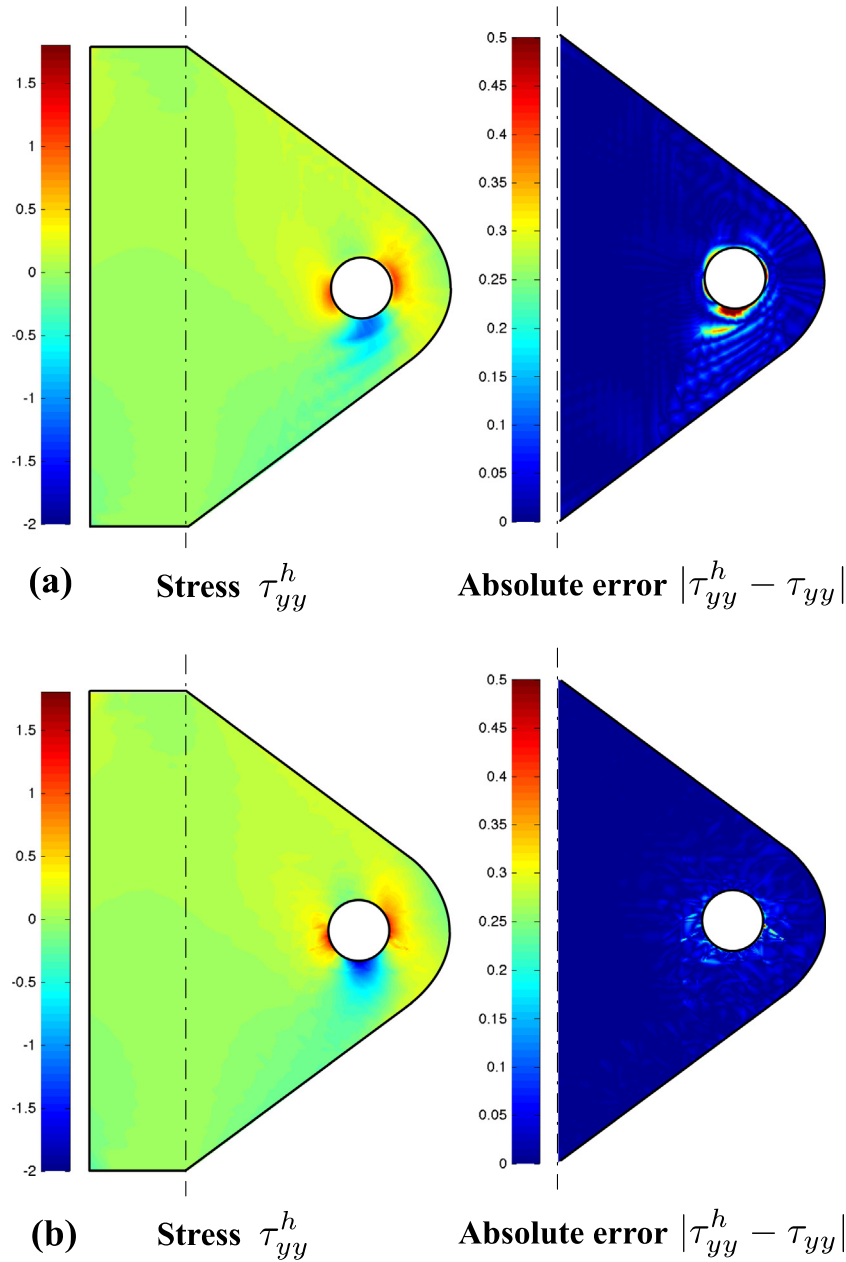


Fig. 25. Stress τ_{yy}^h and absolute error $|\tau_{yy}^h - \tau_{yy}|$; (a) 4-node finite element mesh; (b) new scheme mesh.

quality may decrease with ℓ . Since we measure the calculated strain energy versus the analytical strain energy (given in Eq. (28)) using this coarse mesh, the total error is due to the use of numerical integration and the discretization used, but should be constant with high enough integration order.

Fig. 10 shows the strain energy error of all three methods as a function of the distance ℓ . The solution accuracy of the finite element method enriched by interpolation covers decreases as the mesh is distorted. On the other hand, the results using the overlapping elements and the method of finite spheres are hardly affected by changing ℓ , hence these schemes are less distortion-sensitive. However, as shown in Figs. 10 and 11 the overlapping elements require much less Gauss integration points in the numerical integration, in fact only 5 integration points are needed for each region \mathcal{E}^m while in the method of finite spheres, in each one-dimensional integration domain, many more integration points are required.

3.2. A patch of elements

We consider the patch of elements in Fig. 12 and want to study the accuracy of the strain energy as a function of the number of integration points used per integration domain. For the overlapping elements we use the quadrature rule for the triangular elements [5], and in the method of finite spheres, we use the standard Gauss numerical integration in each quadrant of the disk [17]. In both methods, the displacement field is a rational function, and a high enough integration order must be used.

Fig. 13 shows the accuracy of the strain energy as a function of the number of integration points employed in the integration domains.

As shown in Fig. 13, for a given accuracy, the overlapping elements require much less integration points than the method of finite spheres for which also the required number of integration

points increases very much as the spheres are placed non-uniformly. This sensitivity is not seen when using the overlapping elements for which 6-point integration is sufficient and 9-point integration gives a very small error.

3.3. A cantilever beam analysis using distorted meshes

Our objective is to study the solutions obtained in the analysis of a cantilever beam problem when the mesh using overlapping elements is distorted. Fig. 14 shows the 8 meshes we use, each containing only 8 nodes. We use the quadratic polynomial basis with 9-point integration for the overlapping elements.

Fig. 15 shows the non-smoothed plots of the calculated longitudinal stress τ_{xx} . Table 1 gives the numerical results at selected points of the cantilever beam. To show the performance of the overlapping elements, the percent error ε_h of the strain energy is plotted in Fig. 16. The energy error remains almost constant for all meshes, which indicates that the solutions are quite insensitive to the mesh distortions used, although these are quite high.

3.4. A cantilever plate under uniformly distributed load

The analysis of a cantilever plate is considered to illustrate the application of the overlapping elements in the new paradigm of solution. Fig. 17 shows the plate considered and Fig. 18 shows the discretizations used.

Fig. 19 shows the convergence of the strain energy when h-type uniform refinement is performed (since the displacement field of the overlapping elements is a rational function, in order to reach a higher accuracy, 9-point integration is used in this example). During the mesh refinement using the procedure of the new paradigm of solution, always only two layers of the overlapping elements are used at the plate boundary. The overlapping elements perform very well and indeed better than the discretizations using the finite spheres because the stress boundary conditions are better captured.

4. Using the new paradigm of solution: analysis of a bracket

In this section we present the application of the overlapping elements in the new paradigm of solution by solving the bracket problem already considered in Ref. [2] (see Fig. 20). Our objective is to compare the new solution scheme with a traditional finite element analysis.

Fig. 21 shows the mesh of the new meshing scheme. The inner analysis domain is meshed with the traditional 4-node finite elements and the overlapping elements (with bilinear basis) are used near the boundaries of the bracket and extended to couple with the traditional finite elements. We note that in areas of stress concentrations, like near the hole of the bracket, we can use a finer mesh to improve the solution accuracy.

We solve the bracket problem first with the traditional finite element method using a very fine 9-node element mesh, and use these results as our reference solution, the reference strain energy $E = 1.07$.

In order to compare a traditional finite element analysis with the new paradigm of solution, we solve the bracket problem with 4-node finite elements (see Fig. 22(a)). Table 2 gives the total number of degrees of freedom (DOF), the calculated strain energy and the total number of integration points using the new meshing scheme and the traditional finite element method. We see that the entries given for the two solution approaches are not far apart.

Figs. 23–25 show the resulting stress plots; with e.g. τ_{xx}^h and τ_{xx} denoting the predicted and reference normal stresses corresponding to the x-axis. We see that the new analysis scheme gives

smoother stress fields with smaller absolute stress errors, although a quite distorted mesh is used near the hole of the bracket.

5. Concluding remarks

Our objective in this paper was to present new overlapping elements for the new paradigm of solution of Refs. [1,2]. We gave the basic formulation of the new overlapping elements, including the coupling between these and the traditional finite elements, and studied the performance of the overlapping elements in several numerical examples. The results show two important properties of the new elements: the required numerical integration is much more efficient than in meshfree methods, and the new overlapping elements are quite insensitive to mesh distortions. Then we illustrated the use of the new overlapping elements in the new paradigm of solution of Ref. [2] by solving a cantilever plate problem and a bracket problem.

While the new overlapping elements are very useful and much more efficient than the use of finite spheres, or disks, we realize that to fully harvest the potential of the new paradigm of analysis, more research is needed. For example, the use of the new overlapping elements should be studied in three-dimensional solutions, in the analysis of incompressible media; and they need to be studied in dynamic and wave propagation problems [19,20]. A disadvantage of the overlapping finite elements given in this paper is that they lead to a relatively large bandwidth corresponding to their degrees of freedom. Hence, further studies should also be directed to find even more effective overlapping elements; these would be very valuable for the new paradigm of solution.

References

- [1] Bathe KJ. The finite element method with 'overlapping finite elements'. In: Zingoni A, editor. Proceedings sixth international conference on structural engineering, mechanics and computation – SEMC 2016, Cape Town, South Africa; 2016.
- [2] Bathe KJ, Zhang L. The finite element method with overlapping elements – a new paradigm for CAD driven simulations. *Comput Struct* 2017;182:526–39.
- [3] Bathe KJ. The finite element method. In: Wah B, editor. Encyclopedia of computer science and engineering. J. Wiley and Sons; 2009. p. 1253–64.
- [4] Liu GR. Meshfree methods: moving beyond the finite element method. Taylor & Francis; 2009.
- [5] Bathe KJ. Finite element procedures. Prentice Hall; 1996. 2nd ed. KJ Bathe, Watertown, MA; 2014.
- [6] Dolbow J, Belytschko T. Numerical integration of the Galerkin weak form in meshfree methods. *Comput Mech* 1999;23:219–30.
- [7] Mazzia A, Ferronato M, Pini G, Gambolati G. A comparison of numerical integration rules for the meshless local Petrov-Galerkin method. *Numer Algor* 2007;45:61–74.
- [8] Babuška I, Banerjee U, Osborn JE, Li Q. Quadrature for meshless methods. *Int J Numer Meth Eng* 2008;76:1434–70.
- [9] Babuška I, Banerjee U, Osborn JE, Zhang Q. Effect of numerical integration on meshless methods. *Comput Mech Appl Mech Eng* 2009;198:2886–97.
- [10] Nayroles B, Touzot G, Villon P. Generalizing the finite element method: diffuse approximation and diffuse elements. *Comput Mech* 1992;10:307–18.
- [11] Oden JT, Duarte CA, Zienkiewicz OC. A new cloud-based hp finite element method. *Comput Mech Appl Mech Eng* 1998;153:117–26.
- [12] Strouboulis T, Babuška I, Copps K. The design and analysis of the generalized finite element method. *Comput Mech Appl Mech Eng* 2000;181:43–69.
- [13] Duarte CA, Babuška I, Oden JT. Generalized finite element methods for three dimensional structural mechanics problems. *Comput Struct* 2000;77:215–32.
- [14] Kim J, Bathe KJ. The finite element method enriched by interpolation covers. *Comput Struct* 2013;116:35–49.
- [15] Kim J, Bathe KJ. Towards a procedure to automatically improve finite element solutions by interpolation covers. *Comput Struct* 2014;131:81–97.
- [16] De S, Bathe KJ. The method of finite spheres. *Comput Mech* 2000;25:329–45.
- [17] Lai B, Bathe KJ. The method of finite spheres in three-dimensional linear static analysis. *Comput Struct* 2016;173:161–73.
- [18] Hong JW, Bathe KJ. Coupling and enrichment schemes for finite element and finite sphere discretizations. *Comput Struct* 2005;83:1386–95.
- [19] Ham S, Lai B, Bathe KJ. The method of finite spheres for wave propagation problems. *Comput Struct* 2014;142:1–14.
- [20] Kim KT, Bathe KJ. Transient implicit wave propagation dynamics with the method of finite spheres. *Comput Struct* 2016;173:50–60.